Title

MR Multitasking-based multi-dimensional assessment of cardiovascular system (MT-MACS) with extended spatial coverage and water-fat separation

Journal

Magnetic Resonance in Medicine, 89(4)

ISSN

0740-3194

Authors

Hu, Zhehao
Xiao, Jiayu
Mao, Xianglun
et al.

Publication Date

2023-04-01

DOI

10.1002/mrm.29522

Peer reviewed

Received: 22 June 2022 | Revised: 25 September 2022 | Accepted: 21 October 2022 | Published on: 6 November 2022

DOI: 10.1002/mrm.29522

TECHNICAL NOTE

Magnetic Resonance in Medicine

MR Multitasking-based multi-dimensional assessment of cardiovascular system (MT-MACS) with extended spatial coverage and water-fat separation

Zhehao Hu[1,2,3] | Jiayu Xiao[1] | Xianglun Mao[2] | Yibin Xie[2] | Alan C. Kwan[2,4] | Shlee S. Song[5] | Michael W. Fong[6,7] | Alison G. Wilcox[1] | Debiao Li[2,3] | Anthony G. Christodoulou[2,3] | Zhaoyang Fan[1,2,8,9]

[1]Department of Radiology, University of Southern California, Los Angeles, California, USA

[2]Biomedical Imaging Research Institute, Cedars-Sinai Medical Center, Los Angeles, California, USA

[3]Department of Bioengineering, University of California, Los Angeles, California, USA

[4]Smidt Heart Institute, Cedars-Sinai Medical Center, Los Angeles, California, USA

[5]Department of Neurology, Cedars-Sinai Medical Center, Los Angeles California, USA

[6]Division of Cardiovascular Medicine, University of Southern California, Los Angeles, California, USA

[7]Cardiovascular Thoracic Institute, University of Southern California, Los Angeles, California, USA

[8]Department of Radiation Oncology, University of Southern California, Los Angeles, California, USA

[9]Department of Biomedical Engineering, University of Southern California, Los Angeles, California, USA

Correspondence
Zhaoyang Fan, Department of Radiology, Keck School of Medicine, University of Southern California, 2250 Alcazar Street,

Purpose: To extend the MR MultiTasking-based Multidimensional Assessment of Cardiovascular System (MT-MACS) technique with larger spatial coverage and water-fat separation for comprehensive aortocardiac assessment.

Methods: MT-MACS adopts a low-rank tensor image model for 7D imaging, with three spatial dimensions for volumetric imaging, one cardiac motion dimension for cine imaging, one respiratory motion dimension for free-breathing imaging, one T2-prepared inversion recovery time dimension for multi-contrast assessment, and one T2*-decay time dimension for water-fat separation. Nine healthy subjects were recruited for the 3T study. Overall image quality was scored on bright-blood (BB), dark-blood (DB), and gray-blood (GB) contrasts using a 4-point scale (0-poor to 3-excellent) by two independent readers, and their interreader agreement was evaluated. Myocardial wall thickness and left ventricular ejection fraction (LVEF) were quantified on DB and BB contrasts, respectively. The agreement in these metrics between MT-MACS and conventional breath-held, electrocardiography-triggered 2D sequences were evaluated.

Results: MT-MACS provides both water-only and fat-only images with excellent image quality (average score = 3.725/3.780/3.835/3.890 for BB/DB/GB/fat-only images) and moderate to high interreader agreement (weighted Cohen's kappa value = 0.727/0.668/1.000/1.000 for BB/DB/GB/fat-only images). There were good to excellent agreements in myocardial wall thickness measurements (intraclass correlation coefficients [ICC] = 0.781/0.929/0.680/0.878 for left atria/left ventricle/right atria/right ventricle) and LVEF quantification (ICC = 0.716) between MT-MACS and 2D references. All measurements were within the literature range of healthy subjects.

CSC Room 104, Los Angeles, CA 90033, USA.
Email: zhaoyang.fan@med.usc.edu

Funding information
National Institutes of Health, Grant/Award Number: R01EB028146

Conclusion: The refined MT-MACS technique provides multi-contrast, phase-resolved, and water-fat imaging of the aortocardiac systems and allows evaluation of anatomy and function. Clinical validation is warranted.

KEYWORDS
MR Multitasking, multi-contrast imaging, multi-dimensional imaging, phase-resolved imaging, water-fat separation, whole-heart MR

1 | INTRODUCTION

Cardiovascular diseases, such as congenital heart diseases, cardiac masses (i.e., cardiac thrombi or tumors), and aortic vasculopathy, are common causes of mortality and morbidity globally.[1,2] Diagnosis, risk stratification, and planning of intervention or surgery require accurate evaluation of cardiovascular anatomy and function.[3] As a versatile imaging modality, cardiovascular MR has the potential to provide such a comprehensive assessment. For example, bright-blood (BB) and dark-blood (DB) imaging enables complementary visualization of cardiac chambers and great thoracic vessels,[4] phase-resolved cine imaging is considered the gold standard for assessment of cardiac function,[5] and water-fat separation based on Dixon methods allows additional fat quantification, which could be clinically relevant.[6,7]

Despite the aforementioned benefits, cardiovascular MR is still not widely adopted in current clinical practice.[8] This is mainly owing to three typical challenges: (a) long imaging time associated with the needs for large spatial coverage and high spatial resolution; (b) cumbersome imaging paradigm in which multiple scans, often with non-standard imaging plane prescription, are required for delineating the complex anatomy and function; and (c) nontrivial imaging setup and inefficiency in compensating for cardiac and respiratory motion during data acquisition, such as electrocardiography (ECG) triggering and respiratory navigator gating or breath-holding. Hence, cardiovascular MR is highly time-consuming and dependent on operator experience and patient cooperation.[9]

Multi-dimensional imaging strategies have recently been developed to mitigate the above challenges. Feng et al. proposed a 5D extra-dimensional golden-angle radial sparse parallel (XD-GRASP) framework to achieve whole-heart anatomical evaluation at different cardiac phases.[9] Ginami et al. developed a 3D simultaneous BB and DB phase sensitive (BOOST) to provide complementary image contrasts.[10] More recently, a 3D MR MultiTasking based Multi-dimensional Assessment of Cardiovascular System (MT-MACS) technique has been proposed for multi-contrast, cardiac phase-resolved imaging of the thoracic aorta without the need for ECG triggering or respiratory navigation.[11] Based on the MR Multitasking framework,[12] MT-MACS exploits the image correlation along and across different physiological and physical time dimensions, and thus requires dramatically fewer imaging raw data to resolve multiple overlapping dynamics and construct images with adequate quality.

In this work, we refine the MT-MACS technique from the following aspects. First, the acquisition orientation is switched to a standard coronal view. Unlike the previous oblique sagittal orientation determined using the 3-point tool on localizer images, which requires ECG triggering and several breath-holds, data acquisition in the coronal view gets rid of the complicated localization process and would largely simplify the overall workflow. Second, the spatial coverage and resolution are adapted from $275 \times 220 \times 72\,mm^3$, 1.4 mm isotropic to $224 \times 224 \times 162.4\,mm^3$, interpolated to 1.4 mm isotropic, which achieves comprehensive assessment of not only the thoracic aorta but also the whole heart. Third, we adopt the tiny-golden-angle stack-of-stars k-space trajectory rather than the previous Cartesian sampling. It has been shown that the stack-of-stars trajectory is more motion-robust since the k-space center is densely sampled, which is more suitable in the whole-heart imaging scenario where more complicated cardiac motion is a roadblock. In addition, the tiny-golden-angle scheme is used to reduce the eddy current effects. Last but not least, the water excitation module is replaced by the 2-point Dixon method for fat suppression, where the latter tends to provide sharper images due to reduced echo time and also owns the potential for fat imaging, which could offer another dimension for cardiovascular system assessment. In summary, the newly developed aortocardiac MT-MACS technique allows for ECG- and respiratory navigator-free, multi-dimensional (multiple contrast weightings, cine series, and water-fat images) imaging with a single 10-min scan. We present technical development and a proof-of-concept in vivo study.

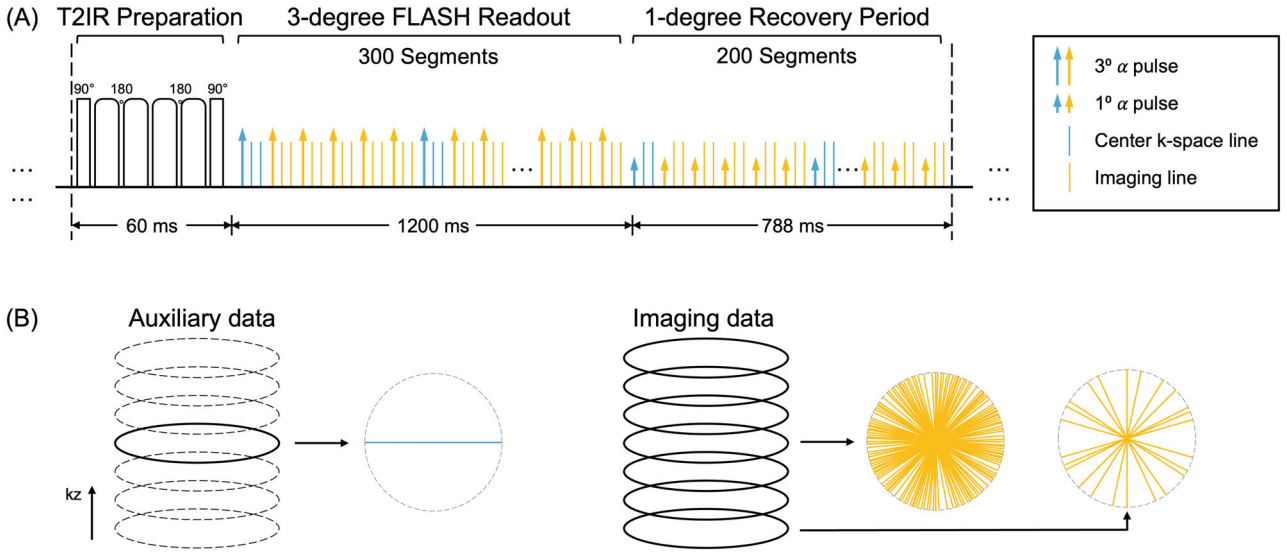

FIGURE 1 Pulse sequence diagram for the MT-MACS technique and corresponding k-space sampling pattern. A, T2-prepared inversion recovery (T2IR) magnetization preparations are applied at constant intervals followed by dual-echo stack-of-stars FLASH readouts. Following each T2IR preparation module, RF pulse flip angles are 3° for the first 300 segments, and 1° for the next 200 segments. Auxiliary data are interleaved with imaging data every six segments. B, Simplified illustration of k-space sampling strategy. The auxiliary data are collected at the 0° radial spoke of the center partition. For the imaging data, randomized partition-encoding reordering following a variable-density Gaussian distribution with the highest density at the center partition adopted in this sequence.

2 | METHODS

2.1 | Pulse sequence design

In this work, the MT-MACS technique was implemented based on continuous dual-echo FLASH readouts with tiny-golden-angle ($\Psi = 32.039°$) stack-of-stars k-space sampling. T2-prepared inversion recovery (T2IR) magnetization preparations are applied at constant intervals to maximize the contrast between myocardium/vessel wall and blood and to create flexible contrast weightings during T1-dominant magnetization recovery.[11] Following each T2IR preparation module, RF pulse flip angles are 3° for the first 300 segments, and 1° for the next 200 segments. Compared to a simple gap used in the recent work,[11] the 1° low-flip-angle excitations are adopted to better track cardiac motion while minimally interfering magnetization recovery. Subspace auxiliary data are interleaved with imaging data every six segments and are collected at the 0° radial spoke of the center partition (Figure 1). Partition-encoding ordering for the imaging data randomized with a variable-density Gaussian distribution with the highest density at the center partition.

2.2 | Image reconstruction framework

The proposed MT-MACS method adopts a low-rank tensor image model for 7D aortocardiac imaging with three spatial dimensions for volumetric imaging, a cardiac phase dimension for phase-resolved cine imaging, a respiratory motion dimension for free-breathing imaging, a T2IR time dimension for multi-contrast assessment, and a T2*-decay time dimension for 2-point Dixon-based water-fat separation. Specifically, a 7D aortocardiac image $I(\boldsymbol{r}, t_c, t_r, t_{T1}, t_E)$ is modeled as a five-way multi-dimensional array (or "tensor") $\mathcal{J}$ with one voxel location dimension $\boldsymbol{r} = [x, y, z]^T$ indexing 3D spatial locations and four time dimensions indexing cardiac motion t_c, respiratory motion t_r, magnetization recovery t_{T1}, and echo time t_E, respectively. High image correlation along and across different time dimensions induces $\mathcal{J}$ to be a low-rank tensor, such that it can be separated in the following sense:

$$\mathcal{J} = \mathcal{C} \times_1 \boldsymbol{U}_{\mathbf{r}} \times_2 \boldsymbol{V}_{t_c} \times_3 \boldsymbol{W}_{t_r} \times_4 \boldsymbol{Y}_{t_{T1}} \times_5 \boldsymbol{Z}_{t_E} \quad (1)$$

where $\times_n$ denotes n-mode multiplication; the columns of factor matrix $\boldsymbol{U}_{\mathbf{r}}$ contain the spatial basis images and the columns of $\boldsymbol{V}_{t_c}$, $\boldsymbol{W}_{t_r}$, $\boldsymbol{Y}_{t_{T1}}$ and $\boldsymbol{Z}_{t_E}$ contain the temporal basis functions for each corresponding time dimension.[13]

Based on the MR Multitasking framework, MT-MACS uses a mixed strategy that reconstructs the image tensor $\mathcal{J}$ by directly recovering the core tensor and different factor matrices, which can be divided into three steps[11,14]:

1. Generate ungated images with one mixed temporal dimension representing elapsed time for image-based cardiac and respiratory phase identification,[12] placing

the corresponding images into 20 cardiac bins and 6 respiratory bins.

2. Determine the inversion recovery basis functions in $\boldsymbol{Y}_{t_{T1}}$ from a pre-generated dictionary of inversion-recovery signals built from the Bloch equations with a range of T1, T2, and B1 inhomogeneity values.
3. Estimate core tensor $\mathcal{C}$ and the basis functions along the cardiac motion, respiratory phase, and echo time dimensions, namely $\boldsymbol{V}_{t_c}$, $\boldsymbol{W}_{t_r}$ and $\boldsymbol{Z}_{t_E}$, respectively, from the high-temporal-resolution auxiliary data. Reconstruct the spatial coefficients $\boldsymbol{U}_{\mathbf{r}}$ by fitting the derived tensor factors to the acquired imaging data.

Detailed multi-dimensional image reconstruction strategies of MT-MACS are shown in Section A of the Supporting Information. The MATLAB (R2018a, MathWorks, Natick, MA) p-code for the reconstruction is available upon request.

2.3 | In vivo study

The in vivo study for proof-of-concept was approved by the local institutional review board, and all subjects provided written informed consent before participation. Nine healthy volunteers (aged 28–79 y, 5 females) were recruited and scanned on a 3T clinical system (MAGNETOM Vida; Siemens Healthcare) with a standard 18-channel body coil and a 32-channel spinal coil.

MT-MACS imaging was prescribed based on an axial scout scan to cover the whole heart and thoracic aorta with no ECG triggering or respiratory navigator. Major imaging parameters were: coronal orientation, FOV = $224 \times 224 \times 162.4\,\text{mm}^3$, acquired spatial resolution = $1.4 \times 1.4 \times 2.8\,\text{mm}^3$ (interpolated to 1.4 mm isotropic), T2 preparation duration = 60 ms, $\text{TR}/\text{TE}_1/\text{TE}_2$ = 3.94/1.23/2.46 ms, bandwidth = 1250 Hz/pixel, total acquisition time = 10.3 min.

In addition, conventional ECG-triggered and end-expiration breath-held sequences were acquired in all subjects to serve as the references for morphological (i.e., myocardial wall thickness for each cardiac chamber) and functional (i.e., left ventricular ejection fraction [LVEF]) quantification of the heart. Specifically, a 2D T2-weighted DB turbo spin-echo (TSE) sequence was performed in a four-chamber orientation with following major imaging parameters: FOV = $360 \times 360\,\text{mm}^2$, matrix size = 256×256, slice thickness = 5 mm, flip angle = 180°, TR = 800 ms, TE = 71 ms, turbo factor = 17, bandwidth = 849 Hz/pixel, ECG-triggered to the mid-diastole, and acquisition time per slice = 14 s. 2D cine imaging based on a segmented balanced SSFP (bSSFP) sequence was performed for 12 contiguous short-axis slices of the left ventricle, with following major imaging parameters: FOV = $300 \times 300\,\text{mm}^2$, matrix size = 224×224, slice thickness = 8 mm, flip angle = 36°, TR/TE = 3.01/1.31 ms, views per segment = 9, bandwidth = 1313 Hz/pixel, 25 phases based on retrospective ECG gating, and acquisition time per slice = 7 s.

2.4 | Image analysis

Images acquired using MT-MACS were reconstructed offline to generate water-only images with multiple contrast weightings (i.e., BB, DB, gray-blood [GB]), and corresponding cine series as well as fat-only images. The DICOM-format MT-MACS images were loaded to a workstation (LEONARDO; Siemens Healthcare) and reformatted to match the 2D reference images in both location and slice thickness. All quantitative analyses were performed using cvi42 version 5.12.1 (Circle Cardiovascular Imaging).

2.4.1 | Qualitative analysis

Subjective image quality assessments of both MT-MACS water-only and fat-only image sets at mid-diastolic end-expiratory phase as well as the corresponding reference sequences were performed by 2 independent radiologists with at least 5 y of experience in cardiovascular imaging. For MT-MACS water-only images, image quality scores were recorded for two anatomic structures (cardiac chambers and thoracic aorta) with three representative image contrasts (BB, DB, and GB). For MT-MACS fat-only images, overall image quality for the entire 3D volume was graded for each image set. The criteria used for the 4-point image quality scale were listed in Section B of the Supporting Information. In addition, to perform depiction assessment of cardiac wall motion, the 3D BB, DB, and GB MT-MACS volumes were reformatted to the short-axis orientation. Temporal fidelity (or blurring) of both MT-MACS and 2D cine balanced SSFP image stacks was graded on a 4-point scale: 1-poor, 2-fair, 3-good, 4-excellent.

2.4.2 | Quantitative analysis

To validate the accuracy of MT-MACS in quantifying morphological parameters of the cardiac chambers, myocardial wall thicknesses of the left atria (LA)/left ventricle (LV)/right atria (RA)/right ventricle (RV) were measured and compared with the conventional reference images. Specifically, myocardial wall thickness of each cardiac chamber was measured at the same location on the DB

images of MT-MACS at the mid-diastolic end-expiratory phase and corresponding matched 2D T2-TSE images, respectively.

For the accuracy analysis of LVEF measurement, the blood-myocardium boundary was manually contoured in each slice of the MT-MACS BB images and corresponding matched 2D cine images for both the end-diastolic and end-systolic phases, respectively. LVEF was then calculated for each sequence using the following equation[15]:

$$\mathrm{LVEF} = \frac{\mathrm{LVEDV} - \mathrm{LVESV}}{\mathrm{LVEDV}} \times 100\% \quad (2)$$

where LVEDV and LVESV represents the end-diastolic and end-systolic left ventricular volume, respectively.

To demonstrate the capability of MT-MACS in fat quantification, manual tracings were performed to measure the fat volume between the myo-epicardial border and visceral-parietal pericardial border.[16] Specifically, the fat volume was contoured on consecutive short-axis slices at the end-diastole phase reformatted from the fat-only images provided by MT-MACS (Figure S1 in Section C of the Supporting Information).

2.5 | Statistical analysis

For qualitative analysis, weighted Cohen's kappa (κ) values were used to evaluate interreader agreement in image quality scoring. For myocardial wall thickness measurements of the LA/LV/RA/RV, a paired two-tailed Student's t-test, intraclass correlation coefficients (ICC), and Bland–Altman analysis were used to measure the difference and agreement between MT-MACS and corresponding matched 2D references. For LVEF measurement, linear regression, ICC, and Bland–Altman analyses were adopted to assess quantification agreement. All statistical analyses were performed in SPSS version 24 (IBM Corp.). A p value <0.05 was considered to indicate statistical significance.

3 | RESULTS

MT-MACS imaging was performed successfully on all subjects. MT-MACS allowed the visualization of both static anatomic and dynamic functional information (Section D of the Supporting Information). Figure 2 shows slices of the ventricular chambers (coronal view and short axis view) and thoracic aorta (candy-cane view) at the mid-diastolic end-expiration phase in two representative healthy subjects. Both water-only and fat-only images generated by MT-MACS are displayed. For water-only images, BB, DB, and GB image contrasts are shown for each slice orientation.

For qualitative analysis, a total of 36 MT-MACS 3D image sets (3 water-only contrasts and 1 fat-only), 9 2D cine balanced SSFP image stacks, and 9 2D T2-TSE slices were scored for image quality. Image quality scores given by both readers are shown in Table 1. For MT-MACS, the interreader agreements quantified by weighted Cohen's kappa were 0.727, 0.609, and 1.000 for BB, DB, and GB at the cardiac chambers; 0.727, 0.727, and 1.000 for BB, DB, and GB at the thoracic aorta; and 1.000 for fat-only images. For reference sequences, the weighted Cohen's kappa values were 0.625 for 2D cine images and 0.438 for 2D T2-TSE. Temporal fidelity scoring was summarized in Table S3 in Section E of the Supporting Information.

An illustration of myocardial wall thickness measurements of the LA/LV/RA/RV is shown in Figure 3A. The thicknesses were measured to be 2.52 ± 0.19 vs 2.43 ± 0.22 mm ($p = 0.437$), 8.99 ± 0.53 vs 8.95 ± 0.68 mm ($p = 0.324$), 2.50 ± 0.21 vs 2.46 ± 0.14 mm ($p = 0.167$), and 4.32 ± 0.78 vs 4.37 ± 0.77 mm ($p = 0.783$) for LA, LV, RA, and RV by MT-MACS and 2D T2-TSE, respectively, which are all within the normal anatomical range.[17–20] The cardiac structures on 2D T2-TSE images from two subjects were substantially blurred due to respiratory motion and were therefore excluded from analysis. Good to excellent agreement in myocardial wall thickness measurements was demonstrated with Bland–Altman plots between MT-MACS and 2D T2-TSE in the remaining seven subjects. The ICCs were 0.781/0.929/0.680/0.878 for LA/LV/RA/RV, respectively (Figure 3B).

Comparison of LVEF measurement between MT-MACS and 2D cine balanced SSFP is displayed in Figure 4. Overall, MT-MACS provided slightly lower LVEF measurements compared with the 2D cine sequence (0.63 ± 0.04 vs 0.66 ± 0.04; regression line: $Y = 1.060\mathrm{X} - 0.075$; $R^2 = 0.855$, $p < 0.001$; ICC = 0.716), which may result from the contrast difference between gradient-echo-based and SSFP-based sequences, but the overall values were still within the physiological range.[21]

For the quantification of fat volume, the measurement result for each subject and corresponding gender, age, and body mass index are shown in Table S2 in Section C of the Supporting Information.

4 | DISCUSSION

Accurate assessment of morphology as well as function of the aortocardiac system is crucial for diagnosis and treatment planning in patients with cardiovascular diseases. Cardiovascular MR is considered the only single imaging modality that can achieve comprehensive assessment.[22] However, cardiovascular MR is still not a first-line study in today's clinical practice, largely due

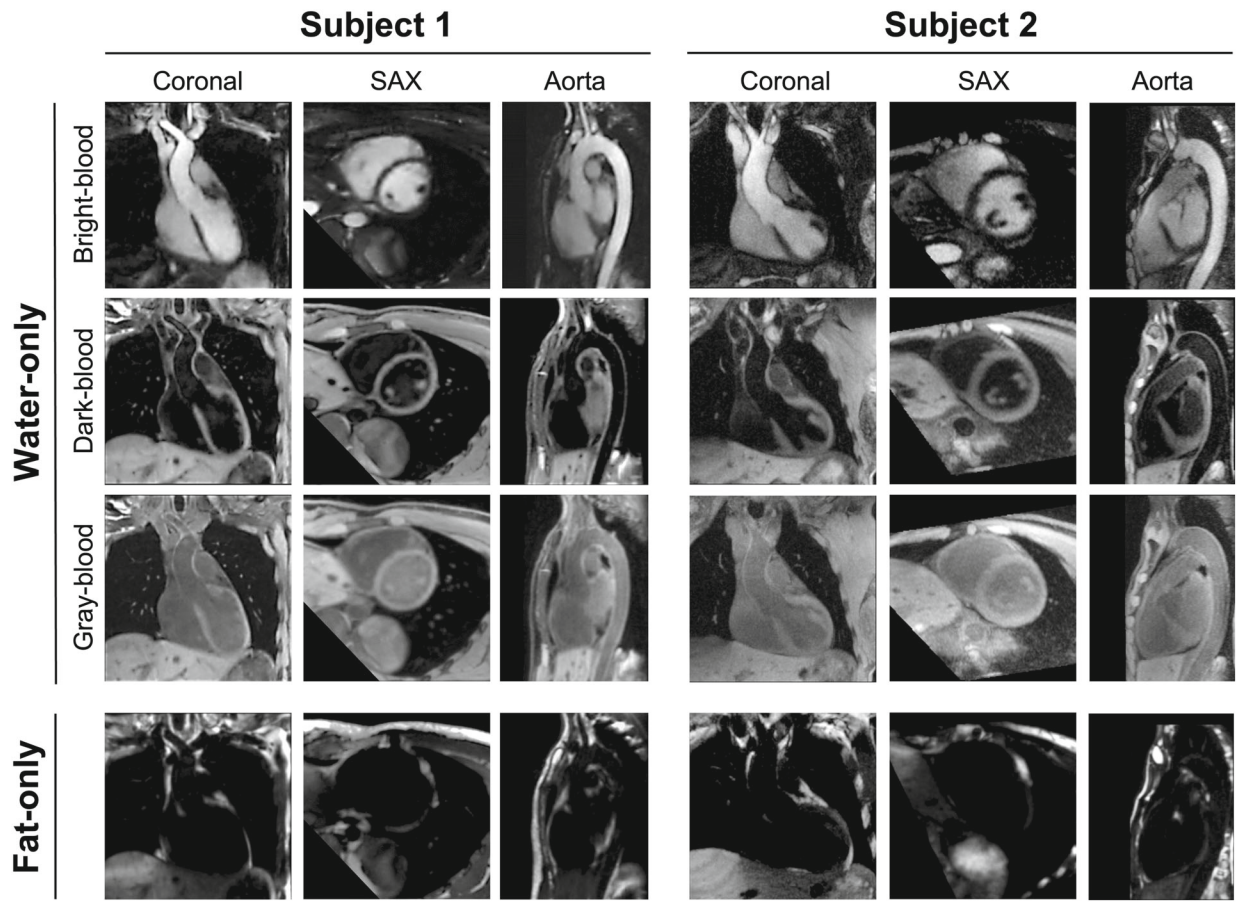

FIGURE 2 Example MT-MACS images of the ventricular chambers (coronal view and short axis [SAX] view) and thoracic aorta at the mid-diastolic end-expiration phase generated from a 28-y-old female subject (Subject 1) and a 65-y-old male subject (Subject 2). Water-only images with multiple contrast weightings, including BB, DB, and GB, and fat-only images are displayed for each slice orientation.

TABLE 1 Image quality scores given by two independent radiologists over all nine healthy subjects

	MT-MACS																	
	Cardiac chambers						Thoracic aorta											
	BB		DB		GB		BB		DB		GB		Fat		2D bSSFP		2D T2-TSE	
	R1	R2	R1	R2	R1	R2	R1	R2	R1	R2	R1	R2	R1	R2	R1	R2	R1	R2
Subject 1	4	4	4	4	4	4	4	4	4	4	4	4	4	4	4	4	4	4
Subject 2	4	4	4	4	4	4	4	4	3	3	4	4	4	4	4	4	4	4
Subject 3	3	3	4	3	4	4	3	3	3	3	4	4	4	4	3	3	1	0
Subject 4	3	3	3	3	4	4	4	4	3	4	3	3	4	4	3	2	1	2
Subject 5	4	3	4	4	4	4	4	4	4	4	4	4	4	4	4	4	4	4
Subject 6	4	4	4	4	4	4	3	4	4	4	4	4	4	4	4	4	4	4
Subject 7	4	4	4	4	4	4	3	3	4	4	4	4	3	3	3	4	4	4
Subject 8	4	4	4	4	4	4	4	4	4	4	4	4	4	4	4	4	4	4
Subject 9	4	4	4	4	3	3	4	4	4	4	3	3	4	4	4	4	4	4
Mean	3.78	3.67	3.89	3.78	3.89	3.89	3.67	3.78	3.67	3.78	3.78	3.78	3.89	3.89	3.78	3.67	3.33	3.33
SD	0.42	0.47	0.31	0.42	0.31	0.31	0.47	0.42	0.47	0.42	0.42	0.42	0.31	0.31	0.63	0.67	1.24	1.33

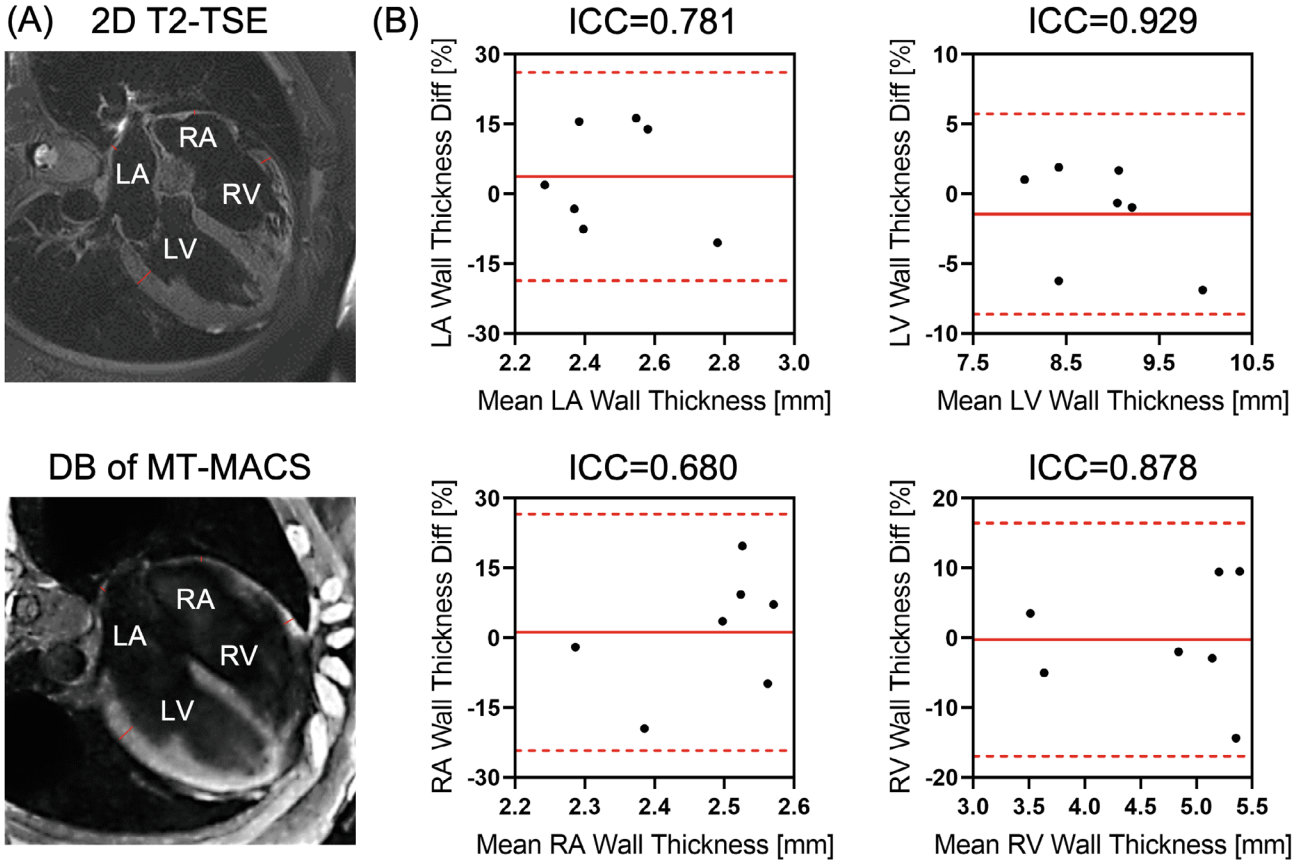

FIGURE 3 Quantification of myocardial wall thickness of the LA/ LV/ RA/ RV. A, Graphic illustration of measuring the myocardial wall thickness of the LA/LV/RA/RV in a 40-y-old male subject. Myocardial wall thickness of each cardiac chamber was measured at the same location on the DB images of MT-MACS at the mid-diastolic end-expiratory phase and corresponding 2D T2-weighted turbo spin-echo images with matched location and slice thickness. B, Bland–Altman plots and ICCs comparing measurement agreements between these two imaging techniques.

to the slow imaging speed and complex clinical workflow.[5,8] To optimize clinical scan time and simplify imaging workflow, in the past few years, various novel comprehensive cardiovascular MR approaches have been developed.[4,9,23–25] Feng et al. proposed a 5D cardiac and respiratory motion-resolved whole-heart imaging technique based on extra-dimensional golden-angle radial sparse parallel (XD-GRASP) framework, which can provide whole-heart anatomical information at different cardiac phases.[9] However, only a single BB image contrast is available through this technique, and this lumenography-based imaging alone may not be optimal in myocardium or vessel wall visualization.[11] To generate complementary image contrasts, a 3D simultaneous BB and black-blood phase sensitive (BOOST) whole-heart MR sequence was developed by Ginami et al.[10] However, the DB volume was retrospectively generated using two differently weighted BB volumes after non-rigid motion correction; thereby any residual motion artifacts would propagate into the black-blood volume leading to image blurring.[4] In addition, the acquisition was ECG-triggered to mid-diastolic resting period and thus cardiac functional parameters cannot be evaluated with this technique.

A novel ECG- and respiratory navigator-free 3D MT-MACS technique was recently published, and its technical feasibility was demonstrated on thoracic aortas.[11] To meet the clinical needs and address the drawbacks of other comprehensive techniques, in this work, we extended the spatial coverage of the previous MT-MACS technique to assess the entire aortocardiac system. Compared with previous comprehensive MR techniques tailored for whole-heart assessment, the proposed method has several advantages. First, MT-MACS provides multiple co-registered images with different image contrast weightings in a single 10.3-min acquisition. A T2IR preparation module was adopted to maximize the contrast between the myocardium/vessel wall and blood while acquiring multiple image contrasts by retrospectively picking out images at different time points along the magnetization recovery time dimension. Specifically, three typical image contrast weightings out of 300 FLASH readout segments were selected, namely BB, DB, and GB image contrasts. In

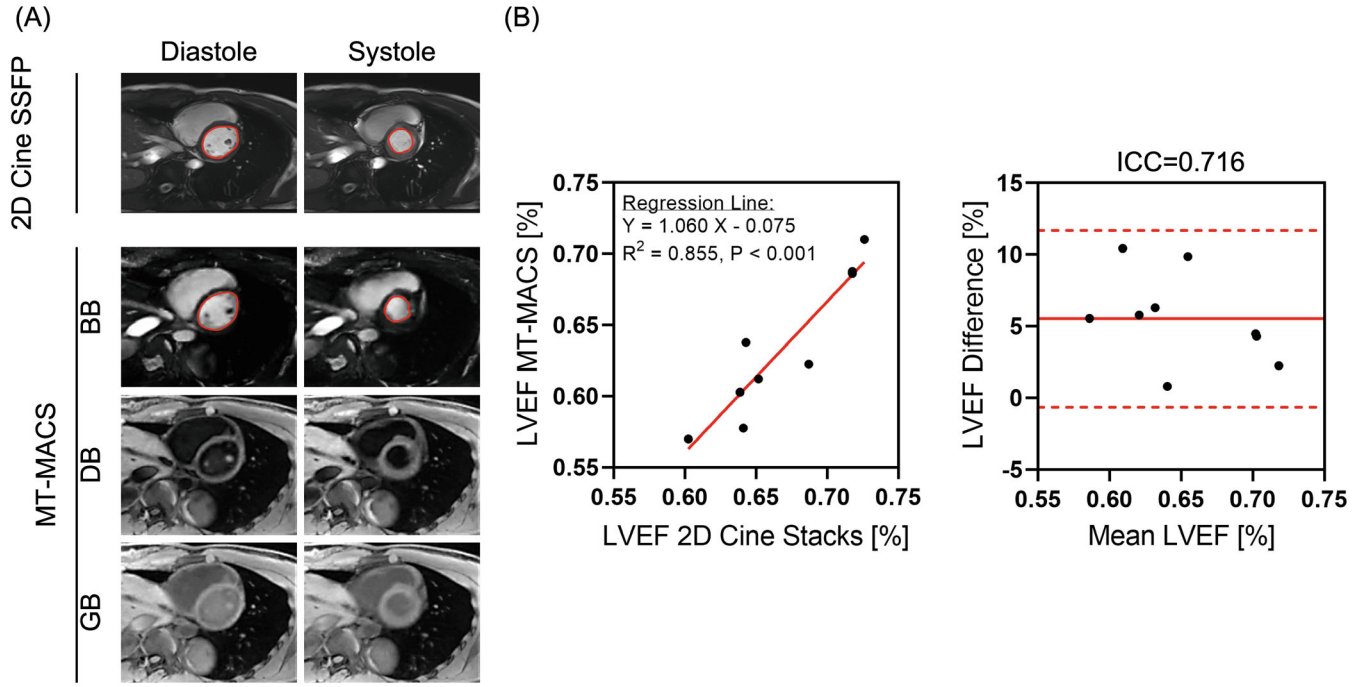

FIGURE 4 Quantification of LVEF. A, Graphic illustration of measuring LVEF in a 39-y-old male subject. The blood-myocardium boundary was manually contoured in each slice of the MT-MACS BB images and corresponding 2D cine balanced SSFP images with matched location and slice thickness for both the end-diastolic and end-systolic phases. B, Linear regression, ICCs, and Bland–Altman analyses comparing the measurement results acquired by these two imaging techniques.

addition, it's worth mentioning that with the T2IR module, the proposed MT-MACS may hold the potential for joint T1/T2 mapping.[26] Second, by adopting a continuous 3D stack-of-stars sampling scheme, MT-MACS eliminates the need for ECG triggering, respiratory navigators, or breath-holds. This greatly improves the acquisition efficiency and reduces the complexity of imaging workflow, and, in the meantime, avoids unreliability or discomfort induced by those external motion compensation methods. Moreover, by unfolding the five-way imaging tensor along the cardiac motion dimension, MT-MACS can provide cardiac phase-resolved cine images for functional imaging (i.e., LVEF quantification), which serves as an important illustration for certain types of cardiovascular diseases.[15] Third, the dual-echo acquisition scheme allows MT-MACS to achieve water-fat separation based on Dixon methods.[27,28] Specifically, by adopting a 2-point Dixon method, MT-MACS potentially has the capability to depict and quantify the relative composition of water and fat in tissues, which could help form a more comprehensive basis for assessment of the cardiovascular system since fat volume has been linked to increased risk of certain cardiovascular diseases.[29]

Our study has some limitations. First, the proposed MT-MACS achieves water-fat separation based on the original 2-point Dixon method, which is under the assumption of perfect B0 field and negligible susceptibility. However, with a shift in B0 field, water and fat will accumulate an additional phase shift, resulting in the mixtures of both water and fat on the final water-only and fat-only images. A possible solution would be to use the extended 2-point Dixon[30] or 3-point Dixon methods.[31] Second, only quantitative metrics of the cardiac chambers were evaluated in this work. This is because the quantitative analyses of the thoracic aorta were performed in our recent work,[11] and we assume the extension here would not adversely impact the aortic delineation in any way. Last, feasibility of the proposed technique requires further validation on patients. The MT-MACS technique could be used to assess various cardiovascular diseases, such as congenital heart diseases and intracardiac thrombus. Such patients need to be recruited to investigate the sensitivity and specificity of diagnosing different types of diseases.

5 | CONCLUSIONS

In this work, we refined the recently developed MT-MACS technique to achieve comprehensive assessment of the aortocardiac system. With a simple imaging setup, MT-MACS allows for multi-dimensional imaging (multiple contrast weightings, cine series, and water-fat images) of the entire heart without the need for ECG triggering, respiratory navigator gating, or breath holding. Further

studies in the setting of various cardiovascular diseases are warranted to validate the clinical utility of this technique.

ACKNOWLEDGMENT

The authors acknowledge research support from the National Institutes of Health (R01EB028146).

ORCID

Zhehao Hu https://orcid.org/0000-0002-5813-2925
Xianglun Mao https://orcid.org/0000-0002-2745-7444
Anthony G. Christodoulou https://orcid.org/0000-0002-9334-8684
Zhaoyang Fan https://orcid.org/0000-0002-2693-0260

TWITTER

Zhaoyang Fan @fan_zhaoyang

REFERENCES

1. Mc Namara K, Alzubaidi H, Jackson JK. Cardiovascular disease as a leading cause of death: how are pharmacists getting involved? *Integr Pharm Res Pract*. 2019;8:1-11.
2. Menchón-Lara R-M, Simmross-Wattenberg F, Casaseca-de-la-Higuera P, Martín-Fernández M, Alberola-López C. Reconstruction techniques for cardiac cine MRI. *Insights Imaging*. 2019;10:1-16.
3. Sakuma H, Takeda K, Higgins CB. Fast magnetic resonance imaging of the heart. *Eur J Radiol*. 1999;29:101-113.
4. Milotta G, Ginami G, Cruz G, Neji R, Prieto C, Botnar RM. Simultaneous 3D whole-heart bright-blood and black blood imaging for cardiovascular anatomy and wall assessment with interleaved T2prep-IR. *Magn Reson Med*. 2019;82:312-325.
5. Mojibian H, Pouraliakbar H. Cardiac magnetic resonance imaging. *Practical Cardiology*. Elsevier; 2022:175-183.
6. Kellman P, Hernando D, Arai AE. Myocardial fat imaging. *Curr Cardiovasc Imaging Rep*. 2010;3:83-91.
7. Eggers H, Brendel B, Duijndam A, Herigault G. Dual-echo Dixon imaging with flexible choice of echo times. *Magn Reson Med*. 2011;65:96-107.
8. Pfeiffer MP, Biederman RW. Cardiac MRI: a general overview with emphasis on current use and indications. *Med Clin*. 2015;99:849-861.
9. Feng L, Coppo S, Piccini D, et al. 5D whole-heart sparse MRI. *Magn Reson Med*. 2018;79:826-838.
10. Ginami G, Neji R, Phinikaridou A, Whitaker J, Botnar RM, Prieto C. Simultaneous bright-and black-blood whole-heart MRI for noncontrast enhanced coronary lumen and thrombus visualization. *Magn Reson Med*. 2018;79:1460-1472.
11. Hu Z, Christodoulou AG, Wang N, et al. Magnetic resonance multitasking for multidimensional assessment of cardiovascular system: development and feasibility study on the thoracic aorta. *Magn Reson Med*. 2020;84:2376-2388.
12. Christodoulou AG, Shaw JL, Nguyen C, et al. Magnetic resonance multitasking for motion-resolved quantitative cardiovascular imaging. *Nat Biomed Eng*. 2018;2:215-226.
13. Kolda TG, Bader BW. Tensor decompositions and applications. *SIAM Rev*. 2009;51:455-500.
14. Shaw JL, Yang Q, Zhou Z, et al. Free-breathing, non-ECG, continuous myocardial T1 mapping with cardiovascular magnetic resonance multitasking. *Magn Reson Med*. 2019;81:2450-2463.
15. Foley TA, Mankad SV, Anavekar NS, et al. Measuring left ventricular ejection fraction-techniques and potential pitfalls. *Eur Cardiol*. 2012;8:108-114.
16. Teme T, Sayegh B, Syed M, Wilber D, Bakhos L, Rabbat M. Quantification of epicardial fat volume using cardiovascular magnetic resonance imaging. *J Cardiovasc Magn Reson*. 2014;16:1-2.
17. Takahashi K, Okumura Y, Watanabe I, et al. Relation between left atrial wall thickness in patients with atrial fibrillation and intracardiac electrogram characteristics and ATP-provoked dormant pulmonary vein conduction. *J Cardiovasc Electrophysiol*. 2015;26:597-605.
18. Bishop M, Rajani R, Plank G, et al. Three-dimensional atrial wall thickness maps to inform catheter ablation procedures for atrial fibrillation. *Europace*. 2016;18:376-383.
19. Yoneyama K, Venkatesh BA, Bluemke DA, McClelland RL, Lima JA. Cardiovascular magnetic resonance in an adult human population: serial observations from the multi-ethnic study of atherosclerosis. *J Cardiovasc Magn Reson*. 2017;19:1-11.
20. Ho S, Nihoyannopoulos P. Anatomy, echocardiography, and normal right ventricular dimensions. *Heart*. 2006;92:i2-i13.
21. Kosaraju A, Goyal A, Grigorova Y, Makaryus AN. *Left ventricular ejection fraction*. In: StatPearls [Internet]. Treasure Island (FL): StatPearls Publishing; 2022.
22. Shah S, Chryssos ED, Parker H. Magnetic resonance imaging: a wealth of cardiovascular information. *Ochsner J*. 2009;9:266-277.
23. Xu J, Kim D, Otazo R, et al. Towards a five-minute comprehensive cardiac MR examination using highly accelerated parallel imaging with a 32-element coil array: feasibility and initial comparative evaluation. *J Magn Reson Imaging*. 2013;38:180-188.
24. Han F, Zhou Z, Han E, et al. Self-gated 4D multiphase, steady-state imaging with contrast enhancement (MUSIC) using rotating cartesian K-space (ROCK): validation in children with congenital heart disease. *Magn Reson Med*. 2017;78:472-483.
25. Ginami G, Lòpez K, Mukherjee RK, et al. Non-contrast enhanced simultaneous 3D whole-heart bright-blood pulmonary veins visualization and black-blood quantification of atrial wall thickness. *Magn Reson Med*. 2019;81:1066-1079.
26. Milotta G, Bustin A, Jaubert O, Neji R, Prieto C, Botnar RM. 3D whole-heart isotropic-resolution motion-compensated joint T1/T2 mapping and water/fat imaging. *Magn Reson Med*. 2020;84:3009-3026.
27. Dixon WT. Simple proton spectroscopic imaging. *Radiology*. 1984;153:189-194.
28. Ma J. Dixon techniques for water and fat imaging. *J Magn Reson Imaging*. 2008;28:543-558.
29. Henningsson M, Brundin M, Scheffel T, Edin C, Viola F, Carlhäll C-J. Quantification of epicardial fat using 3D cine Dixon MRI. *BMC Med Imaging*. 2020;20:1-9.
30. Coombs BD, Szumowski J, Coshow W. Two-point Dixon technique for water-fat signal decomposition with B0 inhomogeneity correction. *Magn Reson Med*. 1997;38:884-889.
31. Wang Y, Li D, Haacke EM, Brown JJ. A three-point Dixon method for water and fat separation using 2D and 3D gradient-echo techniques. *J Magn Reson Imaging*. 1998;8:703-710.

SUPPORTING INFORMATION

Additional supporting information may be found in the online version of the article at the publisher's website.

Table S1. Image quality scoring criteria.
Table S2. Patient characteristics and corresponding fat volume.
Table S3. Temporal fidelity scores given by 2 independent radiologists overall all 9 healthy subjects.
Figure S1. Manual tracings of the fat volume on consecutive short-axis slices (here only base, mid, and apex are displayed as examples) at the end-diastolic phase.

Video S1. Video showing the cardiac motion for water-only bright-blood, dark-blood, and gray-blood image contrast weightings and fat-only images, respectively.

How to cite this article: Hu Z, Xiao J, Mao X, et al. MR Multitasking-based multi-dimensional assessment of cardiovascular system (MT-MACS) with extended spatial coverage and water-fat separation. *Magn Reson Med*. 2023;89:1496-1505. doi: 10.1002/mrm.29522